FISEVIER

Contents lists available at ScienceDirect

## Science of the Total Environment

journal homepage: www.elsevier.com/locate/scitotenv



# Transport of insensitive munitions constituents, NTO, DNAN, RDX, and HMX in runoff and sediment under simulated rainfall



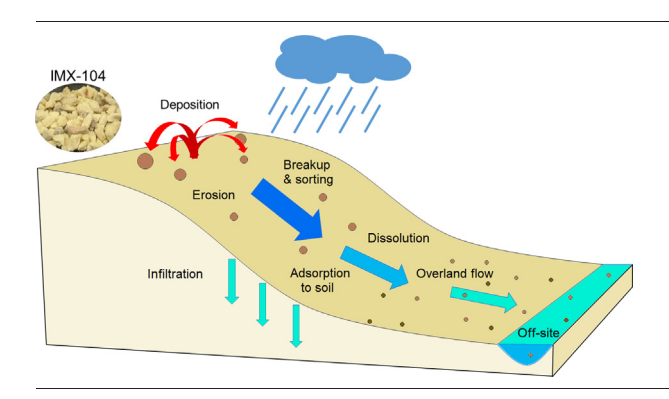
Viktor Polyakov<sup>a,\*</sup>, Warren Kadoya<sup>b</sup>, Samuel Beal<sup>b</sup>, Hayden Morehead<sup>c</sup>, Edward Hunt<sup>d</sup>, Favianna Cubello<sup>c</sup>, Stephen Mercer Meding<sup>d</sup>, Katerina Dontsova<sup>c,d</sup>

- <sup>a</sup> Southwest Watershed Research Center, USDA-ARS, 2000 E Allen Rd, Tucson, AZ 85718, USA
- <sup>b</sup> U.S. Army Engineer Research and Development Center, CRREL, 72 Lyme Road, Hanover, NH 03755-1290, USA
- <sup>c</sup> Department of Environmental Science, The University of Arizona, 1177 E 4th St., Tucson, AZ 85721, USA
- d Biosphere 2, The University of Arizona, 32540 S Biosphere Rd, Oracle, AZ 85623, USA

#### HIGHLIGHTS

- This is the first systematic study of overland transport of IMX-104 under rainfall.
- Runoff and infiltration are primary transport pathways of energetics.
- Energetics mobility is controlled by their fraction size and solubility.
- IMX-104 loss can be predicted using soil sediment yield and energetic fraction.

#### GRAPHICAL ABSTRACT



### ARTICLE INFO

Editor: Dimitra A Lambropoulou

Keywords: Pollutant transport Overland flow Rainfall Insensitive munitions IMX-104

### ABSTRACT

Insensitive munition constituents derived from residues of low order detonations and deposited on military training grounds present environmental risks. A series of rainfall simulation experiments on small soil plots examined the effect of precipitation, soil properties, and particle size on transport of IMX-104 munition components: NTO (3-nitro-1,2,4-triazol-5-one), DNAN (2,4-dinitroanisole), RDX (hexahydro-1,3,5-trinitro-1,3,5-triazine), and HMX (octahydro-1,3,5,7-tertranitro-1,3,5,7-tertranoiro-1,3,5,7-tertranoiro-1,3,5,7-tertranoiro-1,3,5,7-tertranoiro-1,3,5,7-tertranoport in solid form including re-adsorption onto soil particles. The transport was solubility dependent with NTO moving mostly in solution, which was dominated by either runoff or infiltration depending on soil. DNAN, RDX, and HMX, were transported primarily in particulate form. The fine energetic fraction (<2 mm) showed the highest mobility, while the coarsest fraction (>4.75 mm) remained in-situ after rainfall. A simple linear model relating energetics transport with sediment yield and energetics particle size and was proposed. These findings provide the first comprehensive mass balance of munition constituents as affected by overland flow under rainfall. They improve our understanding of environmental fate of munitions, can further be used for predictive model-ling, developing mitigation strategies, and regulatory compliance.

#### 1. Introduction

The US military is introducing new, more stable energetic formulations (IMX-104, IMX-101) in munitions to replace the legacy formulations. During live-fire and testing, the munitions occasionally malfunction, resulting

<sup>\*</sup> Corresponding author.

E-mail address: viktor.polyakov@usda.gov (V. Polyakov).

in incomplete, low-order detonation, which scatters a significant amount of energetic particles on the training grounds (Bigl et al., 2021). Energetics released on the soil surface can pose on-site and off-site environmental hazard due to variable degrees of toxicity (Clausen et al., 2004; Lent et al., 2021). A number of studies examined the spatial distribution, mass, size, and purity of these particles as a function of distance from the origin of detonation (Bigl et al., 2020; Taylor et al., 2015; Walsh et al., 2017a). In the case of IMX-104 these energetic compounds are DNAN (2,4-dinitroanisole), NTO (3-nitro-1,2,4-triazol-5-one), RDX (hexahydro-1,3,5-trinitro-1,3,5-triazine), and HMX (octahydro-1,3,5,7-tertranitro-1,3,5,7-tertrazocine). After deposition, the energetics can potentially move with overland flow in particulate or dissolved form, infiltrate into the subsurface, adsorb onto soil in-situ or onto mobile sediment particles, breakdown when exposed to sunlight, or be taken up by plants (Price et al., 2011).

Dissolution rates of legacy energetic formulations have been previously examined in bulk (Fuller et al., 2012; Lynch et al., 2002; Phelan et al., 2002; Richard and Weidhaas, 2014; Taylor et al., 2015; Taylor et al., 2009) and in relationship with energetic particle sizes (Taylor et al., 2010). IMX-104 is a physical mixture of compounds with solubilities of 16,642 mg  $\rm L^{-1}$ , 276 mg  $\rm L^{-1}$ , 60 mg  $\rm L^{-1}$ , and 5 mg  $\rm L^{-1}$  for NTO, DNAN, RDX, and HMX, respectively (Boddu et al., 2008; Brannon and Pennington, 2002; Spear et al., 1989) and have complex dissolution dynamics. Dontsova et al. (2020b) showed that dissolution rates of IMX-104 can be scaled based on the surface area of the particles. However, determining dissolved transport of IMX-104 in the environment is challenging due to external water fluxes and dynamic solubility limits.

Once mobilized, the IMX-104 compounds can reversibly adsorb to solids from the soil solution or runoff. This process is soil specific, dependent on organic carbon (OC) and/or clay content (Arthur et al., 2017; Boddu et al., 2008; Dontsova et al., 2009; Hawari et al., 2015). DNAN is adsorbed to both OC and clays (Arthur et al., 2017). The adsorption coefficient of energetics ( $K_d$ ) was reported to vary greatly for various soils. Namely, from 0.06 to 8.4 L kg $^{-1}$  for RDX and from 0.09 to 17.7 L kg $^{-1}$  for HMX (Brannon and Pennington, 2002; Tucker et al., 2002).

There is an extensive body of research dedicated to detachment, transport, and deposition of soil sediment by overland flow (Abrahams and Parsons, 1994; Gilley et al., 1985; Takken and Govers, 2000; Zhang et al., 1998). A variety of soil erosion models have been developed to predict soil loss and transport of agricultural contaminants (Borrelli et al., 2021; Nearing et al., 2000). Yet, little is known about the fate of energetics on soil surfaces as affected by hydrological factors, although transport of energetics through soils to the groundwater is relatively well studied (Brannon and Pennington, 2002; Dontsova and Taylor, 2017; Taylor et al., 2017a). This precludes the development of much needed environmental impact prediction tools for energetics similar to those for soil sediment. Currently relevant research is limited to just a few pilot experiments.

Price et al. (2011) investigated the transport of RDX, HMX, and TNT in a flume study under simulated rainfall with a variety of vegetation conditions. The authors reported the attenuation of energetic movement by plants, with TNT being the most affected, and related it to uptake by vegetation. The concentration of energetics in soil declined with the distance from the source. They concluded that the transport of energetics is controlled by a complex interaction of soil properties, plant uptake, and overland flow rates. Fuller et al. (2015) examined the residues of Composition B (Comp B), an energetic containing RDX and TNT, and found that rain drops break up coarse energetic particles into micro particles and thus facilitate faster dissolution. The micro particles, having better mobility, spread across the soil surface in the vicinity of detonation sites. Taylor et al. (2009) examined the behavior of TNT, Tritonal, Comp B and Octol under the impact of water drops, relating their particle size and composition to dissolution rate. They determined that in Comp B, the less soluble RDX controlled the dissolution of TNT.

In order to evaluate precipitation driven transport of IMX-104, and fill related knowledge gaps, we designed a set of rainfall simulation experiments. The objectives of the study were to: a) identify and quantify the primary transport pathways of energetic compounds (NTO, DNAN,

RDX, HMX) in overland flow under simulated rainfall; b) examine the effect of rainfall and particle characteristics on mobility, dissolution, and adsorption of energetics.

#### 2. Methods

#### 2.1. Soil and energetic material

Two soils were used in the experiment. The first, Florence, classified as Laveen loam (coarse-loamy, mixed, superactive, hyperthermic Typic Haplocalcids), was collected in Florence Military Reservation, AZ. The series includes very deep, well-drained soils formed in mixed fan alluvium and characterized by high alkalinity and low organic carbon content (Table 1). The second, Sassafras (loamy, siliceous, mesic Typic Hapudult) was obtained at Aberdeen Proving Ground, MD. Sassafras series is very deep, well drained, moderately permeable soils formed in sandy marine and old alluvial sediments of the Coastal Plain. Both soils were collected from the top 0.15 m layer on uncontaminated by IMX-104 sites, air dried, mixed, and passed through 5 mm sieve.

The IMX-104 particles used for experiments were derived from low-order detonation tests conducted as part of ESTCP project ER18–5105. Tests with IMX-104 (containing NTO, DNAN, RDX (hexahydro-1,3,5-trinitro-1,3,5-triazine) and HMX (octahydro-1,3,5,7-tetranitro-1,3,5,7-tetrazocine) mortar rounds were performed in 2019 on cleared, frozen surfaces at Joint Base Elmendorf-Richardson and at Donnelly Training Area in Alaska following methodology by Walsh et al. (2017b) adapted for low-order detonations. 60-mm and 81-mm IMX-104 mortar rounds were statically detonated using a fuse simulator composed of Composition C-4 (91 % RDX). Particles were collected from the ice surface in 1-m annuli up to 10 m and in 5-m annuli up to 20 m from the point of detonation. The samples were kept frozen until accompanied ice was removed from samples by freeze-drying.

Dry samples were then sieved at 2-mm, and the smaller than 2 mm fraction was analyzed by laser diffraction particle size analysis. Subsequent energetic analysis of the <2 mm particle fraction indicated that the particle purity was dependent on the type of round tested and the distance from detonation. These analyses indicated that larger particle size fractions were pure IMX-104, which were used to generate the purest <2 mm samples to use in this study. Further, the >2-mm particle sizes were passed through 9.51 mm, 4.75 mm, and 2.83 mm sieves. Each fraction was weighed and stored individually (Fig. 1). Care was taken to avoid further breakup during handling. Particles of the 4.75–9.51 mm, 2.83–4.75 mm, and 2.00–2.83 mm fractions with the highest visual purity and <2-mm particles from a detonation with the highest measured energetic purity (86–100 %) were used in rainfall simulation experiments (Bigl et al., 2021).

## 2.2. Experimental setup and instrumentation

The experiment was conducted using four 0.45 m long, 0.32 m wide, and 0.2 m deep stainless steel plots equipped with runoff spillway and three drainage outlets on the bottom (Fig. 1). The latter were connected to a water container via plastic tubing and allowed to collect drainage and control the water table. Plexiglass splash guards were mounted around the perimeter of the plot and four rain gauges were attached, one at each corner.

**Table 1**Physical and chemical properties of soils used in the experiment.

Soil	Texture	Clay %	Silt %	Sand %	pН	EC μS cm <sup>-1</sup>	$\frac{\text{SSA}}{\text{m}^2}$ $\text{g}^{-1}$	OC %	CEC cmol <sub>c</sub> kg <sup>-1</sup>
Florence	Coarse loam	29.0	14.2	56.8	8.3	252	33.0	0.3	13.7
Sassafras	Loam	26.3	6.6	67.1	4.4	148	7.2	1.7	8.9

EC = Electrical Conductivity; SSA = Specific Surface Area; OC = Organic Carbon; CEC = Cation Exchange Capacity (USEPA, 1986).

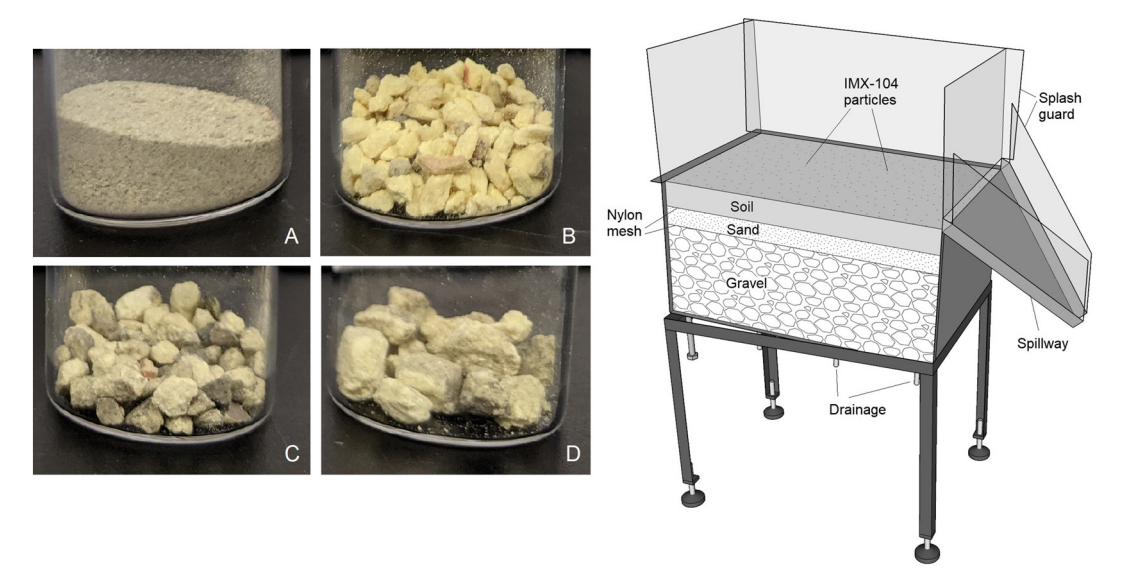


Fig. 1. IMX-104 fractions <2 mm (A), 2.00-2.83 mm (B), 2.83-4.75 mm (C), and 4.75-9.51 mm (D) used in rainfall simulations, and design of the experimental plot.

Rainfall was generated by the Walnut Gulch Rainfall Simulator (WGRS), a portable, computer-controlled, variable intensity simulator with precipitation range of 13 to 180 mm h<sup>-1</sup> (Paige et al., 2004; Polyakov et al., 2018). The WGRS has a single oscillating boom with four V-jet nozzles with overlapping spray pattern. The height of the nozzles is 2.4 m above ground and operating water pressure is 55 kPa. The oscillations are controlled by a stepper motor that varies the speed of boom rotation hence ensuring uniformity of the water application across the plot. The estimated kinetic energy of the rainfall was previously measured to be 204 kJ  $ha^{-1}$  mm<sup>-1</sup>, with a drop size range between 0.29 and 7.2 mm, and a spatial variability coefficient of rainfall distribution of 11 % across the 2 by 6.1 m area. Prior to the experiment the simulator was calibrated over a range of intensities using a set of rain gauges arranged in a grid pattern. This was to ensure that each plot receives the same designed rainfall rate. Reverse osmosis (RO) water was used in experiments to approximate the composition of natural rainfall.

## 2.3. Experimental procedure

The experimental treatments were as follows. Four IMX-104 particle sizes: 4.75–9.51 mm (large, L), 2.83–4.75 mm (medium, M), 2–2.83 mm (small, S), and < 2 mm (extra small, XS); two soils: Florence and Sassafras; and two rainfall intensities: 29.8 and 50.9 mm h $^{-1}$ . Sassafras soil was only tested under 50.9 mm h $^{-1}$  intensity due to higher infiltration capacity and therefore absence of overland flow at lower intensity. Four plots were used simultaneously in a simulation with treatments assigned to them randomly. Each treatment was replicated 3 times for a total of 36 plot-simulations.

The plots were packed with 13 cm of gravel on the bottom, followed by 3 cm of sand to support the water table, and topped with 4 cm of soil. Each component was separated by inert nylon mesh. The soil was filled in three roughly equal layers, compacted after each addition to achieve consistent bulk density, and made flush with the edge of spillway. The weight of soil added was recorded.

Prior to rainfall simulation the plots were positioned horizontally, and the soil was slowly saturated from the bottom through the drainage tubes for about 2 h. Then the plots were positioned at 5 % slope and the water table was lowered to 5 cm below the surface. Once the water table stabilized, 1 g of particles of IMX-104 from one of the fractions was weighed, counted (except the XS fraction), evenly spread on the soil surface, and photographed. The average number of particles per plot was as follows: S 114  $\pm$  14, M 36  $\pm$  8, L 6  $\pm$  1.

Next, simulated rainfall was applied at high (50.9 mm  $h^{-1}$ ) or low (29.8 mm  $h^{-1}$ ) intensity for one hour. Runoff and infiltration samples

were collected at 5 min intervals for a total of 12 samples per plot. Runoff was kept for further analysis, while infiltration samples were weighed and then combined into one cumulative sample per plot. Immediately after the simulation, the soil surface was photographed again. The soil remaining on the plots was then collected in three separate layers (0–1 cm, 1–2 cm, and 2–4 cm). The top layer included any sediment remaining on the spillway and splashguards. The water remaining in the boxes was then drained and subsampled for further analysis. The sand was discarded, and the gravel was removed, washed with RO water and reused

#### 2.4. Laboratory analysis

The runoff samples were weighed to determine the total runoff. Measured runoff was corrected to account for the excess rain water that fell on the spillway (Fig. 1). The samples were processed as follows. On the day of the experiment, a small subsample of the runoff was centrifuged in 30 mL Kimble vials for 20 min at centrifugal force of 3400 g, and the supernatant was filtered using 0.45 µm PVDF syringe filters to obtain Day 1 solution samples. The filtrate was saved and analyzed for energetics compounds using high performance liquid chromatography (HPLC). The next day the remainder of the runoff sample was centrifuged using 750 mL bottles for 20 min at 4700 rpm. Subsamples of the supernatant were filtered through  $0.45~\mu m$  PVDF syringe filter to obtain Day 2 solution samples. These were analyzed for energetic compounds and dissolved organic carbon (DOC), and a subsample was archived. The remainder of supernatant was discarded. Day 1 and Day 2 solution samples were collected because it was not possible to separate sediments from all samples quickly enough on the day of the experiment and particulate IMX-104 in the sediment continued to dissolve over time.

All sediment was transferred into the same glass Kimble vials from Day 1 and centrifuged as described above. The supernatant was discarded, while the sediment was sequentially extracted (Crouch et al., 2019) to determine the total amount of energetics in the sediment. Briefly, methanol was added to the sediment at 5:1 solution to sediment dry weight ratio, equilibrated on a shaker overnight, centrifuged as described above, and decanted. Next, the sediment was extracted using 50:50 (by volume) methanol:water mixture. Both methanol and methanol:water extracts were analyzed by HPLC. The sediment remaining in the vials after extraction was dried at 110 °C overnight and the weight was recorded to determine the total sediment and concentration of the sediment in the runoff.

The top (0-1 cm) bulk soil layer from the plot was air dried, weighed, and ground using puck mill as described in EPA method 8330B

(U. S. Environmental Protection Agency, 2006). This was done to homogenize the sample, which contained a finite number of particles of IMX-104 and could not be representatively subsampled otherwise. After grinding, the samples were extracted as described above for the sediment. The two lower soil layers samples were thoroughly mixed, subsampled and extracted separately without grinding, as no energetic particles were expected at the lower depth. The plot drainage was analyzed by HPLC in the same manner as runoff.

Solution samples, methanol, and methanol:water extracts of the sediment and soils were analyzed using a Dionex Ultimate 3000 HPLC equipped with a diode array detector (ThermoFisher, MA). NTO concentrations (Le Campion et al., 1999) were measured using a Thermo Scientific Hypercarb column, 75:25 acetonitrile:water mobile phase with 0.1 % trifluoroacetic acid (TFA) at 1 mL min $^{-1}$  isocratic for 3 min at 32 °C. NTO was detected at 2.5 min at 315 nm, potential NTO transformation product, 5-amino-1,2,4-triazol-3-one (ATO) set for 220 nm. DNAN, RDX, HMX, and products of DNAN transformation, 2-methoxy-5-nitroaniline and 4-methoxy-5-nitroaniline, were measured using the Thermo Scientific Acclaim reverse phase C18 column, 5  $\mu$ m particle size, 43:57 methanol:water mobile phase with 1 mL min $^{-1}$  flow rate for 30 min. DNAN was detected at 21 min at 300 nm, 2-MeO-5-NA 11 min at 254 nm, 4-MeO-3-NA 6 min at 254 nm, RDX 8 min at 254 nm, and HMX 5 min at 254 nm.

The statistical analysis was performed using SAS 9.4 (SAS, 2008). In all statistical tests P=0.05 was used, unless indicated otherwise.

#### 3. Results and discussion

#### 3.1. Runoff, infiltration, and soil loss

During rainfall simulations a total of 432 runoff samples were collected. Mean rainfall rate was  $29.8\pm2.2\,\mathrm{mm\,h^{-1}}$  for low and  $50.9\pm2.2\,\mathrm{mm\,h^{-1}}$  for high intensity. These approximately correspond to natural events with return frequency of 1-year and 5-year respectively in the Midwest (Hershfield, 1961) as well as Southwest (Polyakov et al., 2010) regions of the US.

The sediment yield, or soil loss, per plot per simulation ranged between 15 g (Sassafras) and 219 g (Florence, 51 mm h $^{-1})$  or an average between 0.08 mm and 1.1 mm of soil loss. No rills or incisions were observed on the soil surface and entire process was considered to be sheet erosion.

On Florence soil (Fig. 2a-b) steady rates of runoff and infiltration were achieved after 10 min of rainfall. Infiltration rate was on average 2.8 mm  $\,h^{-1}$  regardless of rainfall rate. Sediment yield steadily decreased from its peak over the course of the rain by 16 % and 20 % at low and high intensity respectively. This trend was statistically significant and was likely due to preferential removal of finer and loose particles initially and their depletion over time.

Sassafras soil was much more aggregated and exhibited statistically significant temporal trends (Fig. 2c). Runoff increased almost linearly from 7 to 34 mm h $^{-1}$  over 1 h while infiltration decreased from 48 mm h $^{-1}$  (at 15 min peak) to 25 mm h $^{-1}$  at the end. Sediment yield increased steadily over time and was positively correlated with runoff (R $^2=0.55$ ), which is usually its best single predictor (Nearing et al., 2007; Polyakov et al., 2010; Simanton et al., 1993).

#### 3.2. IMX-104 transport in overland flow: solution and particulate

## 3.2.1. Solution

The IMX-104 transport under rainfall differed depending on its initial particle size. The highest concentration of energetics in runoff was observed at the beginning of the rain on plots treated with XS particles (Fig. 3), which dissolved quickly due to their greater specific surface area. Later in the event the runoff concentration in this treatment rapidly decreased to a steady state level and it was more pronounced on Sassafras soil. Similar trend was true for all four IMX-104 components. The concentration in runoff from three larger classes of particles with smaller specific surface

area followed slightly different pattern reaching its peak at 15 to 25 min of rain and then steadily declining (Fig. 3).

This was consistent with previous observations (Dontsova et al., 2020a), where the dissolution rate of energetics was also found to be directly proportional to specific surface area of the particles In addition, smaller particles are transported off site faster leaving less material on the surface to contribute to concentration in runoff later in the event. At the same time larger particles are more likely to remain in place and continue to dissolve into runoff water at lower rate.

Concentrations of four compounds in runoff (Fig. 3 and Appendix 1, 2) depended on their individual solubility: NTO had the largest peak concentrations (410 mg  $\rm L^{-1}$ ), followed by DNAN (39 mg  $\rm L^{-1}$ ), RDX (8 mg  $\rm L^{-1}$ ), and HMX (0.56 mg  $\rm L^{-1}$ ). All observed concentrations were below solubility limits for respective compounds. This indicates that individual IMX-104 constituents within a particle class dissolved independently without inhibition or interference from each other.

The total loss of energetic constituents in solution depended on particle size of energetics. For example, the removal of NTO in dissolved form from Florence soil under 29.8 mm h $^{-1}$  rainfall and XS particle treatment was 39 % of the applied amount, while for L particles it was only 16 % (Table 2). Similar trend was true for three other constituents under both rainfall rates and soils. Overall the percentage loss in solution decreased in the order of NTO, DNAN, HMX, RDX, and from XS to L fraction. The difference between XS and L particle sizes was between 2 and 6 fold depending on the constituent.

On Florence soil the rainfall rate had significant effect on loss in solution of NTO, DNAN, and RDX, but only for XS particles. However, on Sassafras soil a much smaller amount of dissolved energetics was transported comparing to Florence at the same 50.9 mm h $^{-1}$  rainfall rate. This was not only due to lower runoff rate (Fig. 2), but also lower concentration in runoff by approximately a factor of 3 across all four compounds and sizes. The likely reason was that part of the transported mass originated from fine particles or fragments that dissolved before the samples could be analyzed (2–3 h after the collection). Low particle transport rate on Sassafras soil, particularly early in the rainfall event, meant that this specific contribution into Day 1 solution was very small.

## 3.2.2. Particulate

Significant amount of energetics was also transported with sediment, either as particles and their fragments or adsorbed to the surface of the eroded soil (Table 2). Comparison of photos before and after rainfall (Appendix 3) showed that the L particles of energetics typically remained in place, although breakdown and flaking sometimes occurred. The M particles moved short distances downslope but majority of them remained on the plots. The S and XS particles were usually no longer visible on the surface after the rainfall. Often energetic particles were observed in the runoff samples.

The most mobile solid fraction of energetics was XS, where losses of DNAN, RDX, and HMX were between 25 % and 43 % of the input for Florence soil (Table 2, Appendix 4). Losses of NTO for this fraction were 1.3 % to 6.1 % for low and high rainfall intensity respectively. This was due to high solubility of NTO with most of it ending up in solution during transport over the plot or shortly after sample collection. As in the case with dissolved phase, transport rate of solid energetics declined rapidly with increase of particle size for all constituents on both soils and at both rainfall rates. This is consistent with increased ability of rain drops and sheet flow to move particles of smaller size. The peak of solid energetics loss occurred on average at 15-25 min into the rainfall event (Appendix 4, 5, and 6). The dynamics of movement of larger fractions lacked a clear temporal trend, was stochastic in appearance, and had greater variability among replications. This could be attributed to finite number of M and L particles applied to the plot, which caused mass spikes only in selected runoff samples. No significant differences were observed in transport of energetics in sediment in relation to the intensity of rainfall on Florence soil, except NTO and DNAN from XS particle treatment.

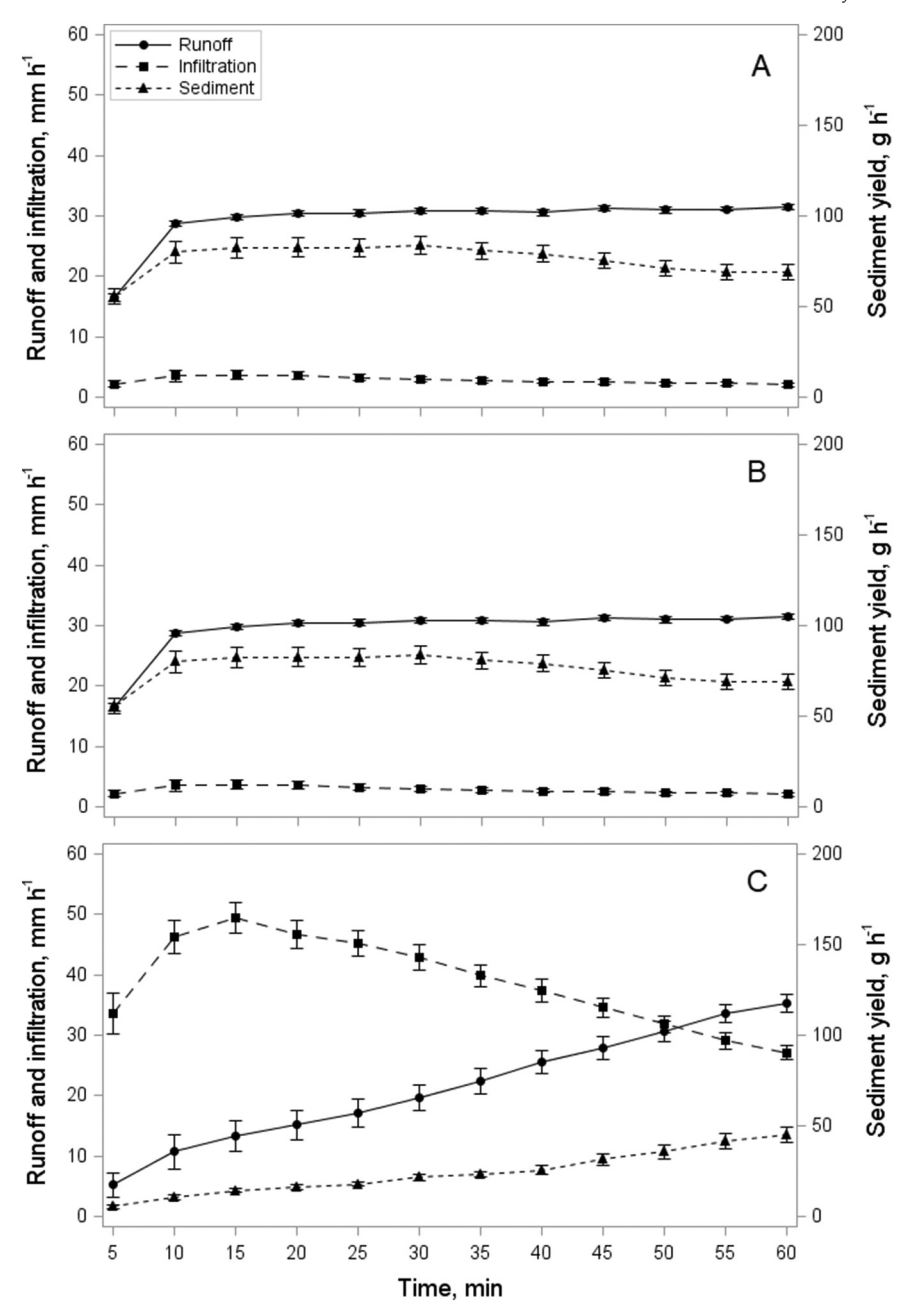


Fig. 2. Runoff, infiltration, and soil loss for Florence soil at 29.8 mm h<sup>-1</sup> (A), Florence soil at 50.9 mm h<sup>-1</sup> (B), and Sassafras soil at 50.9 mm h<sup>-1</sup> rainfall intensity (C). The error bars are confidence interval of the mean (n = 12).

Loss of solid energetics on Sassafras soil was significantly less (2 to 10 fold) than that on Florence at the corresponding rainfall rate, particle sizes, and constituents (Table 2). This difference was statistically significant in all cases, except NTO and DNAN for S and NTO for L particle fractions. This can be explained by smaller transport capacity of overall flow on Sassafras treatment, which itself was due to two factors: lower runoff rate, particularly at the beginning of rainfall event (Fig. 2), and greater surface roughness associated with better aggregation. The latter decreases flow velocity and impedes transport processes (Abrahams et al., 1998; Li et al., 2020).

A portion of the energetics found in runoff sediments was adsorbed to soil particles (Appendix 7). The adsorbed amount was determined based on soil and compound specific adsorption coefficients  $K_d$  (Arthur et al., 2017; Brannon and Pennington, 2002; Mark et al., 2016; Tucker et al., 2002). The highest fraction of adsorbed to the total amount found in sediment was 7.9 % for NTO on Florence soil. This was despite the lowest  $K_d$  (0.06 L  $kg^{-1}$ ) for this compound, and driven by relatively high

concentration of NTO in runoff water. The fraction of adsorbed among DNAN, RDX, and HMX was rather small, between 0.0 % and 1.4 % for both soils (Appendix 7).

The difference between solution concentration on Day 1 and Day 2 (Fig. 4, and Appendix 8 and 9) only confirms that a portion of energetics transport was in the form of undissolved particles or their fragments that continued to dissolve over time releasing IMX-104 constituents into solution. The color of the data points corresponds to the amount of solid energetics present in the sample on Day 1. The concentrations measured in runoff on the second day were noticeably higher for DNAN, RDX, and HMX, but close to 1:1 line for NTO, except for a few samples. In those cases runoff likely contained particles large enough that even more soluble NTO continued to dissolve 24 h after the simulation. Interestingly, this dynamic was also observed even on plots with L particles, which visually remained immobile, indicating that small fragments were breaking off the L particles and moving with runoff.

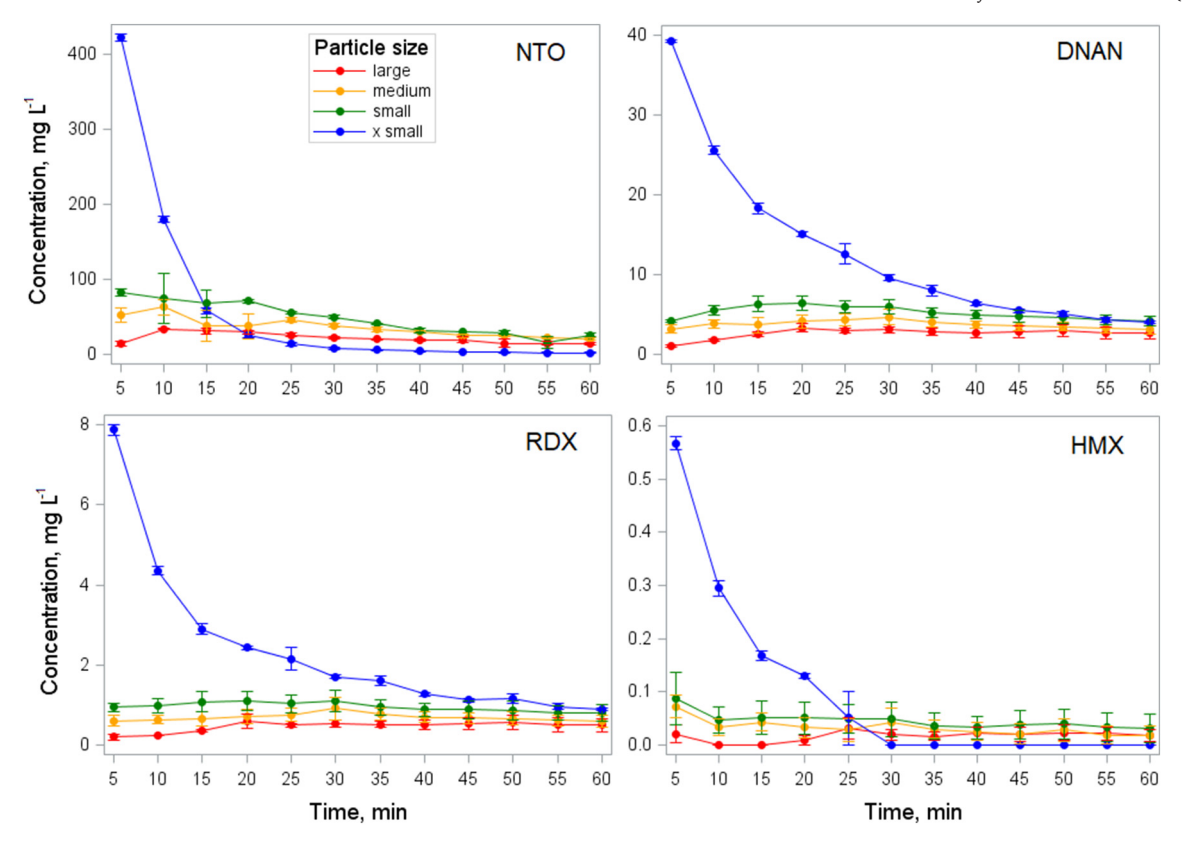


Fig. 3. Concentration of energetic compounds in runoff (Day1) on Florence soil at 29.8 mm h<sup>-1</sup> rainfall rate.

### 3.3. IMX-104 in infiltration and bulk soil

Energetics found in drainage and in soil below 1 cm were considered infiltration losses, assuming that only dissolved energetics could be transported vertically below 1 cm depth. All drainage samples were combined for analysis, hence it is reported as total per rainfall event.

On Florence soil the cumulative infiltration was 2.8 mm per simulation for both rainfall rates. No energetics were found in leachate in the underlying sand. The entire loss to infiltration was contained in the soil between 1 cm and 3 cm depth (Table 2). The loss of NTO to infiltration was 24.8 % on the extra fine particle treatment at 29.8 mm  $h^{-1}$  rainfall rate. It decreased to 4.9 %, 4.9 % and 9.4 % for S, M, and L particle treatments respectively. Interestingly, at a 52 mm h<sup>-1</sup> rainfall the NTO loss rate due to infiltration was smaller: 8.2 %, 0.2 %, 0.2 %, and 0 % respectively for XS to L particle treatments (Table 2). However, these differences between two rainfall treatments were not statistically significant due to very high variability between replications. The possible reason for smaller NTO infiltration losses under greater rainfall is shorter particle residence time, where fines are removed from the surface faster and much of their dissolution takes place off site (in the collection bottle). Among other constituents only a small amount of DNAN (1.6 %) was detected in leachate for S particle treatment under 29.8 mm h<sup>-1</sup> rainfall.

In contrast, Sassafras soil exhibited greater losses of energetics to infiltration, except for HMX, which was not detected in the leachate. It was driven by greater total cumulative infiltration of 38.7 mm per event. The amount of energetic constituents in leachate decreased from XS to L fraction treatment from 60.8 % to 4.4 % for NTO, 11.1 % to 1.1 % for DNAN, and 4.1 % to 0 % for RDX respectively. Only NTO was detected below the soil layer, with this portion of leachate accounting for 55 % of total infiltration losses.

Energetics found in the soil layer between 0 and 1 cm depth were characterized as in situ soil content. Of those most were in particulate form (Appendix 3), although the surface layer contained dissolved and

adsorbed energetics as well. The amount of in situ energetics was positively correlated with particle size increasing from XS to L. Namely, the percentage of the initially applied energetics on Florence soil varied from 37 % to 71 % for NTO, 32 % to 96 % for DNAN, 6 to 87 % for RDX and 4 to 53 % for HMX, with lower value corresponding to XS and upper value to L particle treatment (Table 2). There was no significant difference between in situ energetics under 29.8 mm h $^{-1}$  and 52 mm h $^{-1}$  rainfall with the exception of XS particles for DNAN, RDX, and HMX. This was due to higher mobility of XS particles, which were easily transported by increased overland flow at 52 mm h $^{-1}$  rainfall, while three larger fractions were less affected by it (Appendix 3). On the other hand, in situ NTO from XS particles was unaffected by rainfall treatment because much of it was dissolved regardless of overland flow rate.

In situ retention of energetics on Sassafras soil was slightly larger than that on Florence but not significantly different from it for all particle fractions except XS (Table 2). We did not observe a clear trend of increased retention from S to L particles. However, the in situ content of XS particles was significantly greater on Sassafras than that on Florence for DNAN (75 %), RDX (84 %), and HMX (63 %) and smaller for NTO (3 %). The latter can be explained by greater losses of NTO from XS fraction to infiltration, while the former by rougher Sassafras soil surface and lower runoff rate that prevented easy removal of XS particles in comparison to Florence soil.

It should be noted that in situ energetics are a transient form. Additional pathways in natural conditions include continued mechanical breakup, dissolution by ambient moisture or subsequent rainfall, and photo degradation (Moores et al., 2020; Taylor et al., 2017b).

## 3.4. Total IMX-104 mass balance

The total recovery rate of energetic compounds, on average for both soils was 85 %, 91 %, 87 %, and 60 % for NTO, DNAN, HMX, and RDX respectively. This compares well with previously reported values of 77 %, 104 %, 80 %, and 87 % for the same energetics on several clay loam soils

 Table 2

 Percentage of IMX-104 constituents transported in runoff (dissolved and particulate) depending on soil type and rainfall rate (mean ± confidence interval limit).

Com-pound	Particle size	Dissolved Day1		Sediment		In situ	In situ		Infiltration		Total recovered	
		Mean	±	Mean	±	Mean	±	Mean	±	Mean	±	
Florence, 29.8 n	nm h <sup>-1</sup>											
NTO	x small	38.7	3.6	1.3	0.2	37.2	8.1	24.8	15.4	101.9	4.6	
	small	35.2	2.1	7.0	4.5	43.4	4.8	4.8	6.6	90.4	12.9	
	medium	27.5	7.1	3.7	3.4	58.8	4.5	4.9	9.6	94.9	12.6	
	large	16.4	2.5	0.8	0.6	71.7	39.9	9.4	9.6	98.3	47.8	
DNAN	x small	15.7	1.4	25.7	1.8	31.8	8.5	1.6	1.7	74.9	7.6	
	small	6.6	1.3	11.9	3.1	73.4	18.7	0.0		91.9	19.3	
	medium	4.9	1.4	4.6	1.5	85.4	15.9	0.0		94.8	15.9	
	large	3.4	1.1	2.5	1.0	96.6	73.9	0.0		102.5	75.7	
RDX	x small	6.6	0.7	25.6	1.1	37.7	6.1	1.8	0.4	71.7	5.1	
	small	2.7	1.0	10.3	2.5	73.3	12.9	0.0		86.3	16.1	
	medium	2.1	0.9	4.8	1.2	87.9	45.2	0.0		94.8	44.1	
	large	1.4	0.5	3.2	1.4	87.4	63.9	0.0		92.0	65.8	
HMX	x small	2.4	0.4	25.7	0.3	23.9	4.3	0.0		51.9	4.6	
	small	1.2	1.4	11.5	2.5	38.4	12.0	0.0		51.0	15.9	
	medium	0.9	0.9	5.8	1.3	47.5	15.6	0.0		54.1	15.6	
	large	0.5	0.4	6.4	2.6	53.0	33.2	0.0		59.9	36.3	
	_		***									
Florence, 50.9 n		40.4	4.0	6.1	2.6	24.0	11.6	0.0	10.7	00.7	0.5	
VIO	x small	49.4	4.9	6.1		24.9	11.6	8.2	10.7	88.7	8.5 21.2	
	small	30.0	12.4	4.6	4.4	32.3	7.2	0.2	0.4	67.0		
	medium	29.3	1.8	3.5	2.4	45.8	17.9	0.2	0.2	78.8	14.4	
DNAN	large	11.9	5.4	0.2	0.2	75.1	8.2	0.0		87.2	3.8	
	x small	11.4	1.1	43.1	1.6	13.4	6.1	0.0		67.9	4.4	
	small	5.9	1.5	12.0	7.0	67.8	1.3	0.0		85.7	7.9	
	medium	7.4	2.4	7.0	4.1	81.3	28.8	0.0		95.6	32.8	
	large	3.3	1.3	2.3	0.4	100.0	13.5	0.0		105.7	12.	
RDX	x small	4.5	0.4	24.5	2.4	19.2	4.4	0.0		48.2	2.9	
	small	2.6	1.7	11.8	1.6	63.8	7.9	0.0		78.2	7.0	
	medium	3.9	1.6	9.0	5.2	66.2	23.9	0.0		79.1	25.	
	large	1.7	0.9	3.4	1.1	86.0	15.1	0.0		91.1	15.2	
HMX	x small	1.8	0.3	26.5	2.5	11.5	4.5	0.0		39.9	7.2	
	small	2.1	2.1	14.5	3.4	49.5	17.1	0.0		66.1	20.0	
HMX	medium	3.3	1.8	11.6	4.8	45.2	15.5	8.7	17.1	68.8	29.1	
	large	0.1	0.1	3.6	1.8	64.7	25.9	5.4	10.6	73.9	22.	
Sassafras, 50.9 ı	nm h <sup>-1</sup>											
NTO	x small	8.0	8.3	0.6	0.5	3.1	0.5	60.1	33.6	71.8	25.1	
	small	11.6	8.7	2.5	1.5	48.3	9.8	21.5	13.9	83.9	10.3	
	medium	5.9	1.7	0.5	0.5	62.2	32.0	15.8	4.3	84.5	33.2	
	large	4.0	1.7	0.1	0.1	60.8	4.0	4.4	3.8	69.3	8.0	
DNAN	x small	2.2	1.1	6.1	4.6	74.9	31.7	11.1	5.3	94.4	31.	
	small	1.2	0.5	4.6	2.7	113.0	112.6	0.8	0.8	119.7	115	
	medium	0.7	0.2	1.8	0.8	80.7	33.5	0.1	0.1	83.3	32.	
	large	0.4	0.2	0.9	0.4	76.1	14.1	1.1	1.9	78.4	15.	
RDX	x small	0.9	0.2	7.0	6.0	83.6	22.7	4.1	4.2	95.5	21.	
	small	0.5	0.4	4.2	2.1	117.1	93.5	0.1	0.2	122.0	95.	
	medium	0.3	0.4	2.0	1.0	94.2	47.1	0.0	0.2	96.3	46.	
	large	0.2	0.3	1.1	0.3	94.2 87.4	22.9	0.0		90.3 88.5	23.	
HMX	x small	0.0		6.1	5.5	62.5	12.0	0.0		68.6	10.	
TIVIA												
	small	0.0		2.8	2.1	66.8	31.9	0.0		69.5	33.	
	medium	0.0		1.2	0.5	58.3	28.1	0.0		59.5	27.0	
	large	0.0		0.6	0.5	53.0	15.5	0.0		53.6	15.	

(Crouch et al., 2020) with slightly higher CEC, TOC, and clay content than the ones in our study. Note that in this experiment recovery rates combine both solid and liquid phases. Incomplete recovery could be attributed to extraction and other losses that occurred during sampling and processing. Overall there was no statistically significant relationship between recovery rate and size of applied particles or soil type. Although, recovery of DNAN and RDX from Florence soil decreased slightly for finer energetics fractions.

The pathways of energetics transport depended on their type, fraction size, and soil type (Fig. 5). Most of energetics remained in situ after rainfall, except for XS and S particle fractions. For NTO the primary pathway for off-site transport was infiltration and runoff in dissolved form. These losses varied between 14 % (Florence, L particles) and 95 % (Sassafras, XS particles) and were inversely related to energetic particle size. The loss of NTO for Sassafras was primarily via infiltration, while for Florence it was via surface runoff. Transport of NTO in solid form (sediment) was relatively

small (0.1 % to 8 %) and was due to the fact the particles were either too large to be mobile, or if mobile dissolved fast and moved as solute.

For DNAN, RDX, and HMX the primary off-site loss was due to transport of solid phase in runoff (Fig. 5). For Florence soil it was greater at higher rainfall intensity, was inversely correlated with particle size, and was as high as 63 % for DNAN from XS particles. Relatively low amount of particulate energetics (<7 %) were transported on Sassafras soil, which was consistent with low runoff and sediment yield for that soil especially at the beginning of rainfall event (Fig. 2).

The total combined off-site loss of energetics (solution and sediment) relative to the applied amount on Florence soil was the largest for NTO (40%), followed by DNAN (24%), HMX (17%), and RDX (15%). These are the averages for two rainfall rates, since there was no significant difference between them. For Sassafras the overall off-site loss was smaller and in the following order: NTO (34%) DNAN (8%), RDX (5%), and HMX (3%).

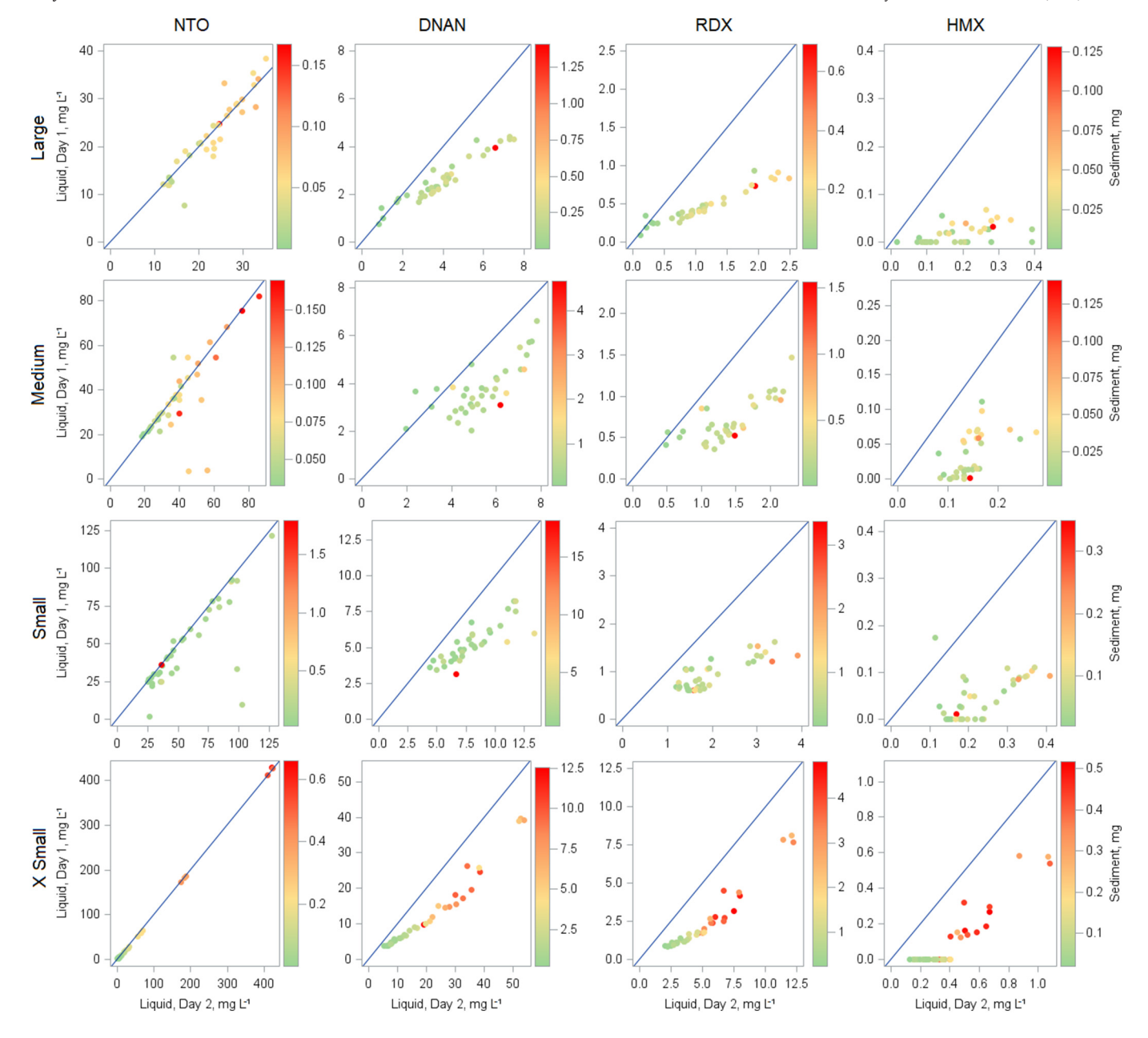


Fig. 4. Concentration dynamics of energetics in runoff samples between Day 1 and Day 2 and energetics remaining in sediment in particulate form (color scale). The samples are from plots with Florence soil subject to 1 h rainfall at 29.8 mm  $h^{-1}$  intensity.

Between the two rainfall intensities on Florence soil, total transport was not statistically different for any of the IMX-104 constituents. This is counter to what we expected, as both dissolution and sediment transport can be expected to increase during rainfall with higher intensity, as total volume of runoff and splash erosion are increased.

## 3.5. IMX-104 transport dynamics

Stepwise selection of predictor variables (SAS, 2008) showed that soil sediment yield and energetic particle size were two best predictors for transport of energetics in runoff. This combination of variables was true for all four compounds. We chose to fit a separate linear model of the following form for each combination of particle size and energetic (Fig. 6 and Appendix 10):

$$E_v = \beta_0 + \beta_1 \times S_v \tag{1}$$

where  $E_y$  is energetics yield per rainfall event, mg;  $S_y$  is sediment yield per event, g;  $\beta_0$  and  $\beta_1$  are linear regression coefficients.

In all of the regressions the relationship was statistically significant at  $\alpha=0.1,$  except for RDX on XS particle treatment (Appendix 10), with  $R^2$  ranging between 0.29 (XS fraction, RDX) and 0.79 (L fraction, RDX). The regression slopes for different size fractions of the same compound were similar, while the intercept was offset, increasing from L to XS size fraction (Fig. 6). Comparison of energetic compounds with one another shows that the regression slopes steadily decreased in the order of NTO, DNAN, RDX, and HMX from approximately 1.0 to 0.01 respectively (Appendix 10). These two regression trends are consistent with our previous observations of total mass balance. Namely, more soluble compounds (NTO) and finer fraction treatments were dominated by transport in dissolved form indicated by high loss of energetics at low soil sediment yield. On the other hand, coarse and less soluble compounds move primarily as particles along with sediment. Hence, at low soil sediment yields energetic transport was also low.

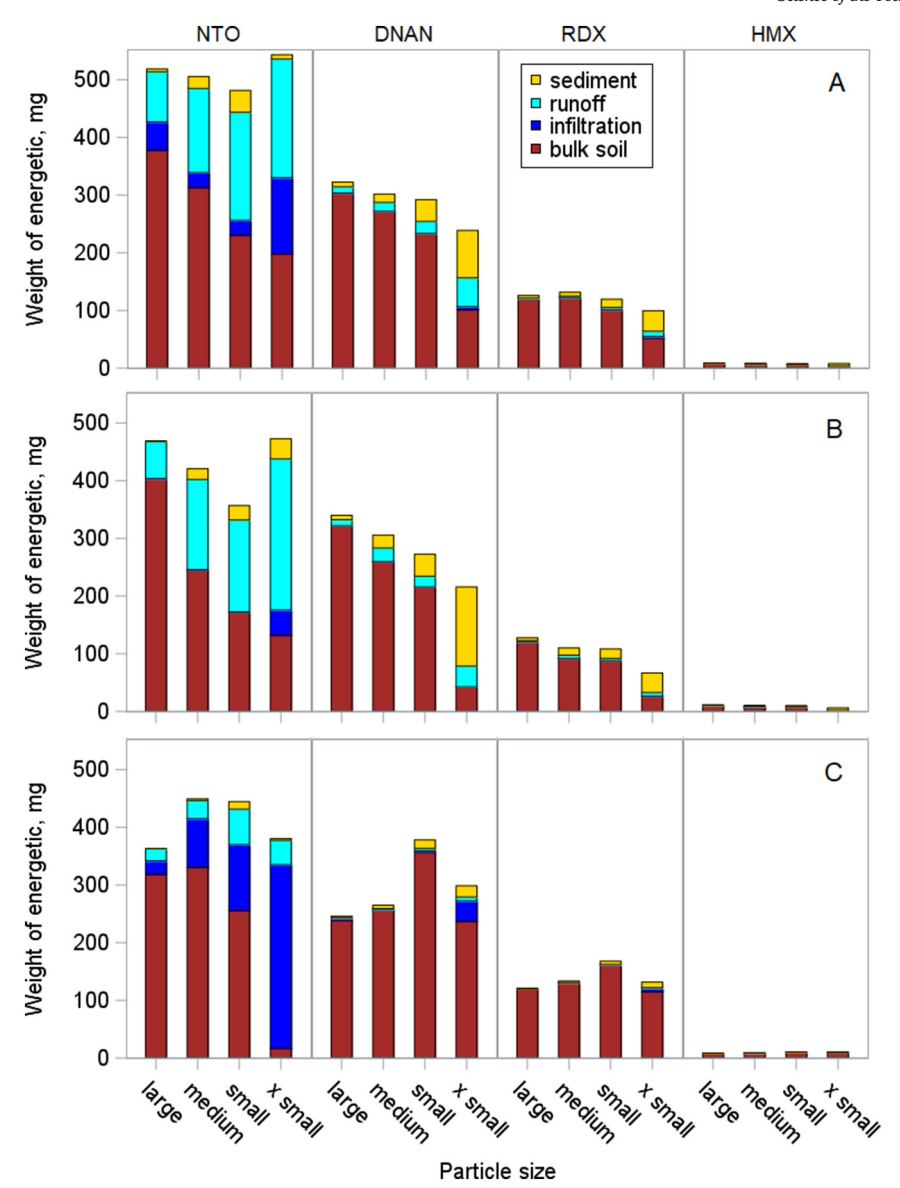


Fig. 5. Total mass balance of IMX-104 by energetic component, pathway, and particle size for Florence soil under 29.8 mm h<sup> $^{-1}$ </sup> (A) and 50.9 mm h<sup> $^{-1}$ </sup> (B), and Sassafras soil under 50.9 mm h<sup> $^{-1}$ </sup> (C) rainfall rates.

Various degrees of solubility is what differentiates energetic and soil sediment transport. For the latter runoff volume or peak are the most common first predictors of yield (Nearing et al., 2007; Polyakov et al., 2010; Simanton et al., 1993). For the former the relationship is more complex, involving dynamic interaction of primary particle movement, breakup, dissolution, re-absorption, and subsurface loss.

## 4. Conclusions

This study is the first effort to systematically quantify detachment and transport of energetic components of IMX-104 in overland flow under rainfall. Three primary pathways for rainfall driven energetic transport were identified: subsurface infiltration, off-site transport in solution, and off-site transport in solid form. The latter included energetics re-adsorbed from solution to soil particles.

Solubility of energetics depended on particle size, with the highest concentration of energetics in runoff observed on plots with XS particle treatment and at the beginning of the rainfall event. The primary transport pathway for NTO was in solution, which could be either surface runoff

(Florence) or infiltration (Sassafras) resulting in over 50 % of NTO being transported off the surface after 51 mm of rainfall. On the other hand, DNAN, RDX, and HMX, were transported primarily in particulate form where the XS fraction (<2 mm) showed the highest mobility. The solid phase losses of this fraction on Florence soil were between 25 % and 43 % of the input for DNAN, RDX, and HMX, while solid phase losses of NTO were 1.3 % to 6.1 %. The loss of solid energetics on Sassafras soil was 2 to 10 fold less than that on Florence due to lower runoff rate. Energetic components with the exception of NTO and fine particles of DNAN, RDX, and HMX remained largely in situ, which in natural conditions would expose them to physical breakup, photo degradation, and dissolution and further transport by subsequent rainfall events.

Transport of energetic compounds was best predicted by soil sediment yield and the size of energetic particles with  $\rm R^2$  ranging from 0.29 to 0.79. The transport process is complex and dynamic process involving interaction of primary particle movement and breakup, dissolution, infiltration, and re-absorption.

Current findings will improve our understanding of the relative importance and contribution of different transport pathways to the fate of

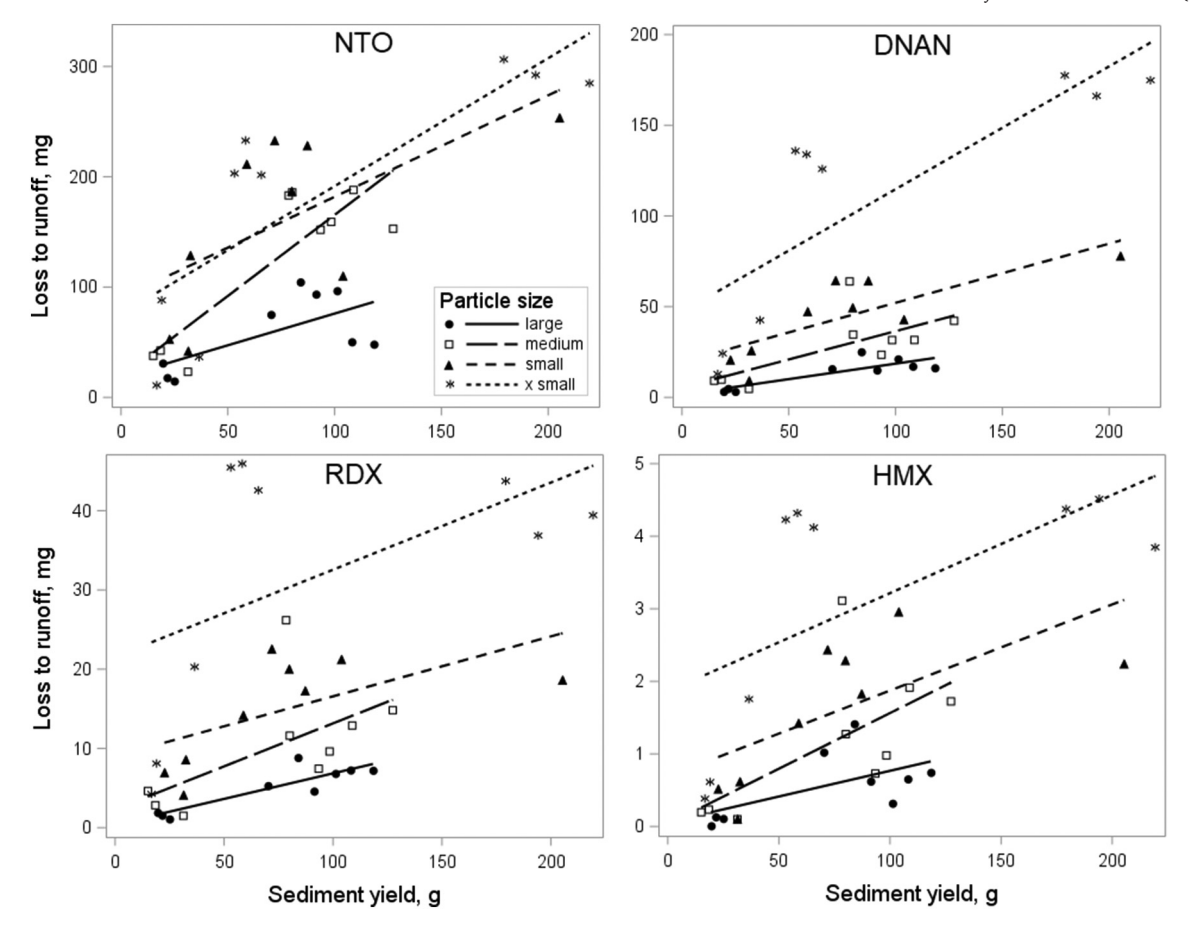


Fig. 6. Loss of energetic compounds (dissolved and particulate) from the plots in runoff as related to sediment yield. Each data point represents one plot-event.

insensitive high explosives. They can be further used to refine models predicting the fate of munitions constituents, assess their environmental impacts, develop mitigation strategies, and meet regulatory requirements.

## CRediT authorship contribution statement

Viktor Polyakov: Writing – original draft, Conceptualization, Methodology, Formal analysis, Investigation, Data curation. Warren Kadoya: Investigation, Resources, Writing – review & editing. Samuel Beal: Investigation, Resources, Writing – review & editing. Hayden Morehead: Investigation, Resources. Edward Hunt: Methodology, Investigation, Resources. Favianna Cubello: Investigation, Resources. Stephen Mercer Meding: Investigation, Resources. Katerina Dontsova: Conceptualization, Methodology, Investigation, Writing – review & editing, Funding acquisition, Supervision.

## Data availability

Data will be made available on request.

### Declaration of competing interest

The authors declare that they have no known competing financial interests or personal relationships that could have appeared to influence the work reported in this paper.

## Acknowledgements

This study was funded through Strategic Environmental Research and Development Program (SERDP) under project ER19-1074. Authors are

grateful to Dr. Andrea Leeson, Deputy Director & Environmental Restoration Program Manager, for continued support; to Kim Birdsall and Dr. Mike Simini for their help in collecting soils used in the experiments; and Matthew Bigl, for providing the energetic residues.

#### Appendix A. Supplementary data

Supplementary data to this article can be found online at https://doi.org/10.1016/j.scitotenv.2023.161434.

## References

Abrahams, A.D., Parsons, A.J., 1994. Hydraulics of interrill overland flow on stone covered desert surfaces. Catena 23 (1–2), 111–140.

Abrahams, A.D., Li, G., Krishnan, C., Atkinson, J.F., 1998. Predicting sediment transport by interrill overland flow on rough surfaces. Earth Surf. Process. Landf. 23 (12), 1087–1099.
 Arthur, J.D., Mark, N.W., Taylor, S., Šimunek, J., Brusseau, M.L., Dontsova, K.M., 2017. Batch soil adsorption and column transport studies of 2,4-dinitroanisole (DNAN) in soils.
 J. Contam. Hydrol. 199, 14–23.

Bigl, M.F., Beal, S.A., Walsh, M.R., Ramsey, C.A., Burch, K.M., 2020. Sieve stack and laser diffraction particle size analysis of IMX-104 low-order detonation particles. ERDC/CRREL TR-20-3. Cold Regions Research and Engineering Laboratory, US.

Bigl, M.F., Beal, S.A., Ramsey, C.A., 2021. Determination of residual low-order detonation particle characteristics from IMX-104 mortar rounds. ERDC/CRREL TR-21-12. US Army Corps of Engineers.

Boddu, V.M., Abburi, K., Maloney, S.W., Damavarapu, R., 2008. Thermophysical properties of an insensitive munitions compound, 2, 4-dinitroanisole. J. Chem. Eng. Data 53 (5), 1120–1125.

Borrelli, P., Alewell, C., Alvarez, P., Anache, J., Baartman, J., Ballabio, C., Bezak, N., Biddoccu, M., Cerdà, A., Chalise, D., 2021. Soil erosion modelling: a global review and statistical analysis. Sci. Total Environ. 780, 146494.

Brannon, J., Pennington, J., 2002. Environmental fate and transport process descriptors for explosives. US, Army Corps Eng., Eng. Res. Dev. Center, Environ. Lab, Vicksburg, MS Final Rep. ERDC/EL TR-02-10.

- Clausen, J., Robb, J., Curry, D., Korte, N., 2004. A case study of contaminants on military ranges: Camp Edwards, MassachusettsUSA. Environ. Pollut. 129 (1), 13–21.
- Crouch, R., Smith, J., Stromer, B., Hubley, C., Beal, S., Lotufo, G., Butler, A., Wynter, M., Ro-Sado, D., Russell, A., Coleman, J., Clausen, J., Giordano, B., Montgomery, M., Bednar, A., 2019. Development and optimization of analytical methods for simultaneous determination of IM and legacy explosive compounds SERDP ER-2722 final report.
- Crouch, R.A., Smith, J.C., Stromer, B.S., Hubley, C.T., Beal, S., Lotufo, G.R., Butler, A.D., Wynter, M.T., Russell, A.L., Coleman, J.G., 2020. Methods for simultaneous determination of legacy and insensitive munition (IM) constituents in aqueous, soil/sediment, and tissue matrices. Talanta 217, 121008.
- Dontsova, K., Taylor, S., 2017. High explosives: their dissolution and fate in soils. In: Shukla, M., Boddu, V., Steevens, J., Reddy, D., Leszczynski, J. (Eds.), Energetic Materials: From Cradle to Grave. Springer, pp. 373–406.
- Dontsova, K.M., Hayes, C., Pennington, J.C., Porter, B., 2009. Sorption of high explosives to water dispersible clay: influence of organic carbon, aluminosilicate clay, and extractable iron. J. Environ. Oual. 38 (4), 1458–1465.
- Dontsova, K., Taylor, S., Qin, C., Hunt, E., Brusseau, M., Simunek, J., 2020. Photo-transformation, sorption, transport, and fate of mixtures of NTO, DNAN, and traditional explosives as a function of climatic conditions (ER-2727). 2020 SERDP & ESTCP Symposium, November 30 December 4. 2020. Virtual.
- Dontsova, K., Taylor, S., Qin, C., Hunt, E., Brusseau, M., Simunek, J., 2020. Photo-transformation, sorption, transport, and fate of mixtures of NTO, DNAN, and traditional explosives as a function of climatic conditions (ER-2727). SERDP & ESTCP Symposium, Nov. 30 Dec. 4, Virtual.
- Fuller, M.E., Schaefer, C.E., Andaya, C., Lazouskaya, V., Fallis, S., Wang, C., Jin, Y., 2012. Dissolution kinetics of sub-millimeter composition B detonation residues: role of particle size and particle wetting. Chemosphere 88 (5), 591–597.
- Fuller, M.E., Schaefer, C.E., Andaya, C., Fallis, S., 2015. Production of particulate composition B during simulated weathering of larger detonation residues. J. Hazard. Mater. 283, 1–6.
- Gilley, J.E., Woolhiser, D.A., McWhorter, D.B., 1985. Interrill soil-erosion .1. Development of model-equations. Trans. ASAE 28 (1) 147-&amp.
- Hawari, J., Monteil-Rivera, F., Perreault, N., Halasz, A., Paquet, L., Radovic-Hrapovic, Z., Deschamps, S., Thiboutot, S., Ampleman, G., 2015. Environmental fate of 2, 4dinitroanisole (DNAN) and its reduced products. Chemosphere 119, 16–23.
- Hershfield, D.M., 1961. Rainfall Frequency Atlas of the United States for Durations from 30 Minutes to 24 Hours and Return Periods From I to 100 Years. Cooperative Studies Section, Hydrologic Services Division for Engineering Division, Soil Conservation Service, U.S. Department of Agriculture, Washington, DC.
- Le Campion, L., Giannotti, C., Ouazzani, J., 1999. Photocatalytic degradation of 5-nitro-1,2,4-triazol-3-one NTO in aqueous suspention of TiO2. Comparison with Fenton oxidation. Chemosphere 38 (7), 1561–1570.
- Lent, E.M., Leach, G., Johnson, M.S., 2021. Development of health-based environmental screening levels for insensitive munitions constituents. Hum. Ecol. Risk. Assess. 27 (6), 1543–1567.
- Li, L., Nearing, M., Polyakov, V., Nichols, M., Cavanaugh, M.L., 2020. Evolution of rock cover, surface roughness, and flow velocity on stony soil under simulated rainfall. J. Soil Water Conserv. 75 (5), 651–668.
- Lynch, J.C., Brannon, J.M., Delfino, J.J., 2002. Dissolution rates of three high explosive compounds: TNT, RDX, and HMX. Chemosphere 47 (7), 725–734.
- Mark, N., Arthur, J., Dontsova, K.M., Brusseau, M., Taylor, S., 2016. Adsorption and attenuation behavior of 3-nitro-1,2,4-triazol-5-one (NTO) in eleven soils. Chemosphere 144, 1249–1255.
- Moores, L.C., Jones, S.J., George, G.W., Henderson, D.L., Schutt, T.C., 2020. Photo degradation kinetics of insensitive munitions constituents nitroguanidine, nitrotriazolone, and dinitroanisole in natural waters. J. Photochem. Photobiol. A Chem. 386, 112094.
- Nearing, M.A., Romkens, M.J.M., Norton, L.D., Stott, D.E., Rhoton, F.E., Laflen, J.M., Flanagan, D.C., Alonso, C.V., Binger, R.L., Dabney, S.M., Doering, O.C., Huang, C.H., McGregor, K.C., Simon, A., 2000. Measurements and models of soil loss rates. Science 290 (5495), 1300–1301.

- Nearing, M.A., Nichols, M.H., Stone, J.J., Renard, K.G., Simanton, J.R., 2007. Sediment yields from unit-source semiarid watersheds at walnut gulch. Water Resour. Res. 43 (6), W06426 06410.01029/02006WR005692.
- Paige, G.B., Stone, J.J., Smith, J.R., Kennedy, J.R., 2004. The walnut gulch rainfall simulator: a computer-controlled variable intensity rainfall simulator. Appl. Eng. Agric. 20 (1), 25–31.
- Phelan, J.M., Romero, J.V., Barnett, J.L., Parker, D.R., 2002. Solubility and dissolution kinetics of composition B explosive in water. SAND Report SAND2002-2420. Sandia National Laboratories, Albuquerque, NM.
- Polyakov, V.O., Nearing, M.A., Nichols, M.H., Scott, R.L., Stone, J.J., McClaran, M.P., 2010. Long-term runoff and sediment yields from small semiarid watersheds in southern Arizona. Water Resour. Res. 46.
- Polyakov, V., Stone, J., Collins, C.H., Nearing, M.A., Paige, G., Buono, J., Gomez-Pond, R.L., 2018. Rainfall simulation experiments in the southwestern USA using the walnut gulch rainfall simulator. Earth Syst. Sci. Data 10 (1), 19–26.
- Price, R.A., Bourne, M., Price, C.L., Lindsay, J., Cole, J., 2011. Transport of RDX and TNT from composition-B explosive during simulated rainfall. American Chemical Society ACS Symposium Series, pp. 229–240.
- Richard, T., Weidhaas, J., 2014. Dissolution, sorption, and phytoremediation of IMX-101 explosive formulation constituents: 2, 4-dinitroanisole (DNAN), 3-nitro-1, 2, 4-triazol-5-one (NTO), and nitroguanidine. J. Hazard. Mater. 280, 561–569.
- Sas, 2008. SAS/STAT® 9.2 User's Guide. SAS Institute Inc., Cary, NC.
- Simanton, J.R., Osterkamp, W.R., Renard, K.G., 1993. Sediment yield in a semiarid basin: Sampling equipment impacts. In: Hadley, R.F., Mizuyama, T. (Eds.), Sediment Problems: Strategies for Monitoring. Prediction and Control, IAHS, pp. 3–9.
- Spear, R.J., Louey, C.N., Wolfson, M.G., 1989. A preliminary assessment of 3-nitro-1, 2, 4-triazol-5-one (NTO) as an insensitive high explosive. Materials Research Labs, Australia.
- Takken, I., Govers, G., 2000. Hydraulics of interrill overland flow on rough, bare soil surfaces. Earth Surf. Process. Landf. 25 (13), 1387–1402.
- Taylor, S., Lever, J.H., Fadden, J., Perron, N., Packer, B., 2009. Simulated rainfall-driven dissolution of TNT, Tritonal, Comp B and Octol particles. Chemosphere 75 (8), 1074–1081.
- Taylor, S., Lever, J., Walsh, M., Fadden, J., Perron, N., Bigl, S., Spanggord, R., Curnow, M., Packer, B., 2010. Dissolution rate, weathering mechanics, and friability of TNT, Comp B, Tritonal, and Octol, ERDC CRRL 147-& Description of the companion of the c
- Taylor, S., Dontsova, K., Walsh, M.E., Walsh, M.R., 2015. Outdoor dissolution of detonation residues of three insensitive munitions (IM) formulations. Chemosphere 134, 250–256.
- Taylor, S., Dontsova, K., Walsh, M., 2017a. Insensitive munitions formulations: their dissolution and fate in soils. In: Shukla, M., Boddu, V., Steevens, J., Reddy, D., Leszczynski, J. (Eds.), Energetic Materials: From Cradle to Grave. Springer, pp. 407–443.
- Taylor, S., Walsh, M.E., Becher, J.B., Ringelberg, D.B., Mannes, P.Z., Gribble, G.W., 2017b.Photo-degradation of 2,4-dinitroanisole (DNAN): an emerging munitions compound.Chemosphere 167, 193–203.
- Tucker, W.A., Murphy, G.J., Arenberg, E.D., 2002. Adsorption of RDX to soil with low organic carbon: laboratory results, field observations, remedial implications. Soil Sediment Contam. Int. J. 11 (6), 809–826.
- U. S. Environmental Protection Agency, 2006. SW846 method 8330b. Nitroaromatics, nitramines, and nitrate esters by high performance liquid chromatography (HPLC). Office of Solid Waste and Emergency Response, Washington, DC.
- Usepa, 1986. Cation-exchange Capacity of Soils (Sodium Acetate), SW846 Method 9081. Office of Solid Waste and Emergency Response, Washington, DC.
- Walsh, M., Thiboutot, S., Gullette, B., 2017a. Characterization of residues from the detonation of insensitive munitions. SERDP Project ER-2219, 3–17.
- Walsh, M.R., Temple, T., Bigl, M.F., Tshabalala, S.F., Mai, N., Ladyman, M., 2017b. Investigation of energetic particle distribution from high-order detonations of munitions. Propellants, Explos., Pyrotech. 42 (8), 932–941.
- Zhang, X.C., Nearing, M.A., Miller, W.P., Norton, L.D., West, L.T., 1998. Modelling interrill sediment delivery. Soil Sci. Soc. Am. J. 62 (2), 438–444.